Radar-Based Predictive Network Management for RIS-Aided THz Communications in Industrial Environments

Francesco Miccoli*, Mattia Fabiani#*, Giampaolo Cuozzo*, Gianni Pasolini#*, Davide Dardari#*
#DEI, Università di Bologna, Italy
*National Laboratory of Wireless Communications (WiLab), CNIT, Italy

***Abstract*—THz communications offer ultra-high data rates and low latency, making them well-suited to meet the emerging Industrial Internet of Things (IIoT) applications, but suffer from blockage events. A promising solution is the deployment of Reconfigurable Intelligent Surfaces (RISs), albeit at the cost of complex management and configuration. To address this challenge, this paper proposes an algorithm that proactively configures the network (i.e., Base Station (BS) and RISs) based on sensing data obtained from a MIMO radar co-located with the BS. Network-level simulations in a dynamic industrial environment demonstrate the effectiveness of our approach compared to an ideal oracle with perfect localization.**

***Index Terms*—Terahertz (THz), Reconfigurable Intelligent Surfaces (RISs), Frequency-Modulated Continuous Wave (FMCW), Radar, Localization, Predictive Network Management.**

I. Introduction

The fourth industrial revolution, also known as Industry 4.0, is enriching the manufacturing world through Information and Communications Technologies (ICT). In particular, the Industrial Internet-of-Things (IIoT) is one of the key enablers of the Industry 4.0 paradigm, as it connects a vast network of sensors, actuators, and autonomous systems to enhance the efficiency, automation, and performance of industrial processes. This paradigm also unleashes the rise of innovative real-time services, such as Extended Reality (XR)-based maintenance, remote monitoring, and digital twins, which enable real-time simulation and optimization of industrial processes [1].

The stringent requirements of these next-generation use cases [2] make TeraHertz (THz) wireless systems particularly attractive, as THz communications, operating in the 0.1–10 THz frequency range, promise to enable ultra-high data rates while supporting low-latency and high-capacity connectivity. However, despite their potential, THz signals face three major challenges: (i) their short wavelengths lead to complete signal blockage by obstacles, making Non-Line-of-Sight (NLoS) communication unfeasible; (ii) high frequencies result in severe path loss and atmospheric absorption, significantly limiting coverage; and (iii) the need for highly directional antennas to mitigate propagation loss increases the risk of beam misalignment, degrading overall performance [3].

A promising approach to mitigating NLoS limitations in THz-based IIoT systems is the deployment of Reconfigurable Intelligent Surfaces (RISs). These devices consist of digitally reconfigurable elements capable of reflecting the incident wave in the desired direction, varying the characteristics of the impinging waves [4]. They can be installed on walls and provide a low-cost solution to bypass possible obstacles, creating alternative links between communicating devices. However, the adoption of RIS technology presents significant challenges, particularly in their real-time configuration and management.

For example, in [5], the authors try to enhance the narrow-beam scanning procedure by using larger beams for initial alignment and iteratively searching for the optimal RIS configuration. However, this approach is impractical in dynamic scenarios due to latency constraints. Other works, such as [6] and [7], address IIoT-specific challenges, like coverage enhancement and device-RIS association, proposing joint device-RIS association algorithms to optimize configurations under both perfect and imperfect Channel State Information (CSI). However, these solutions rely on theoretical analyses without accounting for real-world complexities. The survey [7] reviews various beam tracking and channel estimation methods for RIS-based THz systems, including iterative algorithms and machine learning approaches. It also highlights the potential of sensing and localization at THz frequencies for millimetric precision, but notes that this remains a significant challenge due to the large number of antenna elements required. In [8], a tutorial on integrating radiofrequency sensing and localization with RIS is presented, but it focuses solely on static scenarios, emphasizing the need for advanced techniques in dynamic environments.

Hence, to the best of the authors' knowledge, no existing work leverages localization to optimize beam management and RIS configuration in dynamic environments. In addition, in IIoT scenarios, communication outages due to delayed blockage detection can be intolerable. The duration of communication outages can be reduced by increasing the localization rate, but this is not always feasible. To fill this gap, this paper proposes a novel approach that exploits radar-based localization data to predict the blockage event, which corresponds to NLoS condition, before it occurs and proactively configure both the BS and the RISs, ensuring reliable communication links at THz frequencies despite blockages caused by moving objects. We validate our solution through network-level simulations of uplink data communications between User Equipments (UEs) and the BS in a dynamic industrial scenario.

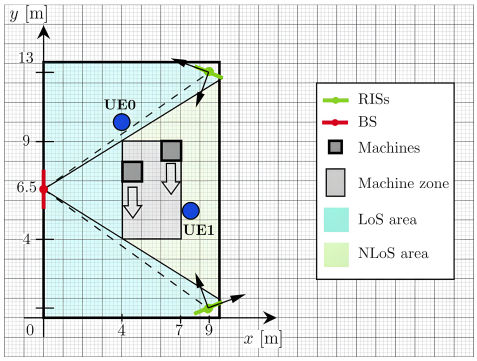

Fig. 1: The considered industrial scenario.

II. Scenario

Although the proposed approach is general, for the sake of explanation and performance assessment, we refer to a specific industrial scenario. It consists of a 2D industrial environment measuring 9m × 13m, whose layout is depicted on the left-hand side of Fig. 1. We assume that broadband cellular connectivity is provided in this area by a Base Station (BS) operating at 300 GHz, serving two stationary User Equipments (UEs), namely UE0 and UE1. These devices may represent, for instance, sensing units collecting data to be forwarded to a control center monitoring ongoing industrial processes.

Two moving machines (e.g., pallet conveyors) are also considered, represented by dark grey boxes in Fig. 1. These machines follow a straight trajectory from the top to the bottom of the light grey area highlighted in the same figure, referred to as the machine zone, which measures 3m × 5m. With this setup, UE0 always maintains a Line-of-Sight (LoS) connection with the BS, whereas UE1 initially has a LoS link but later experiences blockages due to the movement of the machines.

To avoid connectivity failures, two RISs are strategically positioned to maintain LoS links with the BS at all times, while also providing LoS coverage to areas that may be shadowed by the moving machinery, ensuring continuous connectivity between the BS and UE1 when the direct link is unavailable.

Fig. 1 also highlights, using distinct colors, the area where a LoS link can always be established between the BS and the UEs, as well as the area where this condition might be lost, potentially requiring the activation of the most suitable RIS among the two positioned in the top-right and bottom-right corners.

III. Radar-based localization at THz frequencies

To acquire information on the industrial environment, the BS employs a Frequency-Modulated Continuous-Wave (FMCW) radar with a single transmit antenna and M_{r} receive antennas, operating at a carrier frequency f_c. The radar periodically transmits a burst of chirp signals to sense the surrounding environment. The received signal is mixed with the transmitted signal to produce an Intermediate Frequency (IF) signal containing frequency and phase differences. The data cube $\mathbf{X} \in \mathbb{C}^{S \times M_r \times N}$ is a three-dimensional tensor representing raw radar data: S is the number of samples per chirp, M_r is the number of receive antennas, and N is the number of chirps per frame. It is obtained by sampling the IF signal at rate f_s with an analog-to-digital converter to get S samples per chirp.

From the raw radar data $\mathbf{X} \in \mathbb{C}^{S \times M_{\mathrm{r}} \times N}$, a Fast Fourier Transform (FFT) is performed across all dimensions of $\mathbf{X}$. The FFT along the first dimension (fast-time) transforms the IF signal into the frequency domain, yielding the beat frequency $f_b = \mu\tau$, where $\mu = B/T_c$ is the chirp slope, B is the bandwidth, T_c is the chirp duration, and $\tau = 2r/c$ is the round-trip delay for a target at range r, with c being the speed of light. The range is then computed as $r = cf_b/(2\mu)$. Next, an FFT across the chirp dimension (slow-time) resolves the Doppler shift f_d, enabling radial velocity calculation via $v = cf_d/(2f_c)$, where f_c is the carrier frequency. Finally, an FFT across the antenna dimension extracts phase differences, providing azimuth angular information. Then, range-Doppler and range-azimuth maps can be constructed for target localization.

A distance-dependent threshold is applied to the radar maps to produce a detection point cloud. This is achieved using an exponential decay threshold defined as $\gamma = \gamma_0 e^{-\alpha r}$, where γ_0 is the initial threshold value, r is the target range, and α is a tunable parameter to adjust the threshold's sensitivity to distance. Range-azimuth and range-Doppler point clouds are merged based on common range, ensuring target distinction when they are close in angle but differ in velocity, or vice versa. We employ Density-Based Spatial Clustering of Applications with Noise (DBSCAN) [9] to cluster targets by density. DBSCAN uses two main parameters: *epsilon* and *min_pts*. *Min_pts* sets the minimum number of detected points to declare a valid cluster.

A Kalman filter is applied to track the positions of detected targets over time. The Kalman filter, implemented with a state vector $[x, y, v_x, v_y]^T$, initialized with positions from the first radar frame and velocities derived from positional differences. The state transition matrix F incorporates a finer time step than the radar update rate. By denoting I_n as a $n \times n$ identity matrix, the measurement matrix H observes the position, with process noise covariance $Q = \sigma_q I_4$ and measurement noise covariance $R = \sigma_r I_2$, where σ_q and σ_r are tuned parameters. The filter predicts positions at each fine step, updating every radar measurement with radar centroids. The resulting fine-grained data include positions, velocities, and sizes for each detected target. Additionally, a LoS blockage check is conducted at each step, leveraging bounding box vertices of detected machines to evaluate obstructions between the BS and each UE, updating the blockage condition accordingly.

IV. RIS-based Communication at THz Frequencies

In this section, we describe how we model the radio channel between K single-antenna UEs, M RISs comprising $N_{\mathrm{m}} = N_{\mathrm{m,x}} \times N_{\mathrm{m,y}}$ elements, and a BS equipped with an antenna array of N_{r} elements.

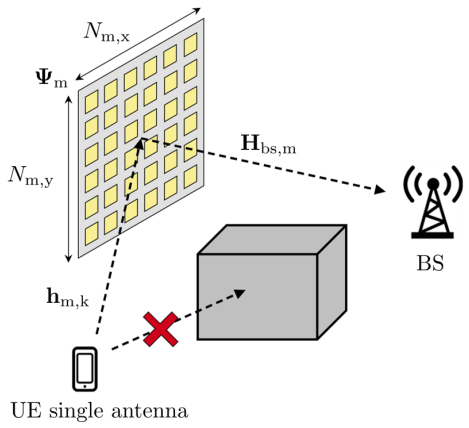

Fig. 2: Representation of the UE-RIS-BS link in case of a blockage event.

UE-BS radio channel modeling: The channel vector $\mathbf{h}_{\mathrm{k}} \in \mathbb{C}^{N_{\mathrm{r}} \times 1}$ for the k-th UE-BS link considers free space propagation between each transmitting and receiving antenna element. This assumption is justified for THz communications, where highly selective beamforming in LoS conditions makes the free-space model a valid approximation. The generic element of the channel vector is thus defined as:

$$h_{\mathrm{k,n}} = \sqrt{G_{\mathrm{k}} G_{\mathrm{n}}} \frac{\lambda}{4\pi d_{\mathrm{k,n}}} e^{-\mathrm{j}\frac{2\pi}{\lambda} d_{\mathrm{k,n}}}, \tag{1}$$

with $h_{\mathrm{k,n}}$ representing the channel coefficient between the k-th UE and the n-th BS antenna element, $d_{\mathrm{k,n}}$ denoting the Euclidean distance, λ is the wavelength, G_{k} and G_{n} are the gain of the elements of the UE and BS, respectively. In our channel model, if the direct path is obstructed, the signal is assumed to be completely lost, resulting in a null $\mathbf{h}_{\mathrm{k}}$.

UE-RIS-BS radio channel modeling: The channel vector $\mathbf{h}_{\mathrm{k}}$ that characterizes the UE-RIS-BS link for the k-th UE and the m-th RIS ($m \in \{1, ..., M\}$) is expressed as follows:

$$\mathbf{h}_{\mathrm{k}} = \mathbf{H}_{\mathrm{bs,m}} \mathbf{\Psi}_{\mathrm{m}} \mathbf{h}_{\mathrm{m,k}}, \tag{2}$$

where $\mathbf{h}_{\mathrm{m,k}} \in \mathbb{C}^{N_{\mathrm{m}} \times 1}$ is the channel vector between the k-th UE and the m-th RIS, $\mathbf{H}_{\mathrm{bs,m}} \in \mathbb{C}^{N_{\mathrm{r}} \times N_{\mathrm{m}}}$ is the channel matrix between the BS and the RIS, while $\mathbf{\Psi}_{\mathrm{m}} \in \mathbb{C}^{N_{\mathrm{m}} \times N_{\mathrm{m}}}$ denotes the scattering matrix of the m-th RIS. Specifically, we model the RISs with a single connected architecture, which means that $\mathbf{\Psi}_{\mathrm{m}}$ can be written as:

$$\mathbf{\Psi}_{\mathrm{m}} = \mathrm{diag}(e^{-\mathrm{j}\psi_{\mathrm{m},1}}, e^{-\mathrm{j}\psi_{\mathrm{m},2}}, ..., e^{-\mathrm{j}\psi_{\mathrm{m},N_{\mathrm{m}}}}), \tag{3}$$

where $\psi_{\mathrm{m}} \triangleq (\psi_1, \psi_2, ..., \psi_{N_{\mathrm{m}}})$ is the vector of the phase shifts. Each RIS is assigned with a codebook of vectors $\psi_{\mathrm{m}}(\Theta_{\mathrm{inc}}, \Theta_{\mathrm{ref}})$, where the incident angle is $\Theta_{\mathrm{inc}} = (\theta_{\mathrm{inc}}, \phi_{\mathrm{inc}})$ and the reflective angle is $\Theta_{\mathrm{ref}} = (\theta_{\mathrm{ref}}, \phi_{\mathrm{ref}})$[1]. Assuming a fixed Θ_{ref} for the RIS-BS link and dividing both the elevation and azimuth planes into 90 discrete angles, a codebook of 90×90 phase shift vectors can be computed [10] for each possible Θ_{inc} in the UE-RIS link. We say that the RIS is *activated* when one of the possible ψ_{m} is chosen.

[1]Assuming the conventional spherical coordinate system, the azimuth and elevation angles are defined as: $\phi \in [0, 2\pi)$ and $\theta \in [0, \pi)$, respectively.

Based on the relative positions of UEs, RISs, obstacles, and the BS, the radio channel vector $\mathbf{h}_{\mathrm{k}}$, which models the direct or indirect link between the k-th UE and the BS, falls into three cases: (i) a direct UE-BS path exists, and each element of $\mathbf{h}_{\mathrm{k}}$ follows (1); (ii) due to obstructions, only an indirect UE-RIS-BS path is available if the RIS is properly configured (as illustrated in Fig. 2), in which case $\mathbf{h}_{\mathrm{k}}$ follows (2); (iii) both direct and indirect paths coexist, resulting in an overall channel vector given by the sum of the respective components.

Given $\mathbf{h}_{\mathrm{k}}$, it is possible to compute the signal-to-interference-plus-noise ratio (SINR) for each $k \in \{1, ..., K\}$, where we assume the Maximum Ratio Combining (MRC) technique at the receiver. In particular, the expression of $\mathrm{SINR}_{\mathrm{k}}$ is as follows:

$$\mathrm{SINR}_{\mathrm{k}} = \frac{\|\mathbf{h}_{\mathrm{k}}\|^2 P_{\mathrm{k}}}{\sigma_{\mathrm{w}}^2 + I}, \tag{4}$$

where the numerator represents the useful received power from the k-th UE that transmits with power P_{k}, σ_{w}^2 is the thermal noise power, and the interference power I is given by

$$I = \sum_{\mathrm{i} \neq \mathrm{k}}^{K} \left| \frac{\mathbf{h}_{\mathrm{k}}}{\|\mathbf{h}_{\mathrm{k}}\|} \mathbf{h}_{\mathrm{i}} \right|^2 P_{\mathrm{i}}, \tag{5}$$

where P_{i} is the transmit power of the i-th interfering UEs, $\|\mathbf{h}_{\mathrm{k}}\|$ denotes the norm of the channel vector $\mathbf{h}_{\mathrm{k}}$, while $|\cdot|^2$ represents the square modulus; under the assumption that both noise and interference follow a Gaussian distribution.

Figure 3 illustrates an example of the uplink SINR spatial distribution for a single UE-RIS-BS link within the considered scenario (see Sec. II) with parameters listed in Table I. The results show that, with an appropriate configuration of $\mathbf{\Psi}_{\mathrm{m}}$, the coverage can be significantly extended behind the machine zone, achieving an SINR range of 8–15 dB within a $3\mathrm{m}^2$ region in proximity to the RIS.

V. Proposed Approach

In this section, we present the proposed algorithm for predictive network management at THz frequencies, where both the BS and RISs are proactively configured based on localization information provided by the radar mounted on the BS. Specifically, with a periodicity of τ, the radar provides estimates of the coordinates and dimensions of detected targets, which are subsequently classified as either machines or UEs based on their respective sizes: if the largest dimension is less than 1 m, the target is classified as a UE; otherwise, it is identified as a machine. Using this estimated scenario information, the MRC precoding vector at the BS for a k-th UE can be computed as

$$\mathbf{v}_{\mathrm{k}} = \frac{\mathbf{h}_{\mathrm{k}}^{\mathrm{H}}}{\|\mathbf{h}_{\mathrm{k}}\|}, \tag{6}$$

with $\mathbf{h}_{\mathrm{k}}$ given by (2) by assuming perfect CSI estimation. Additionally, based on the estimated positions of the targets,

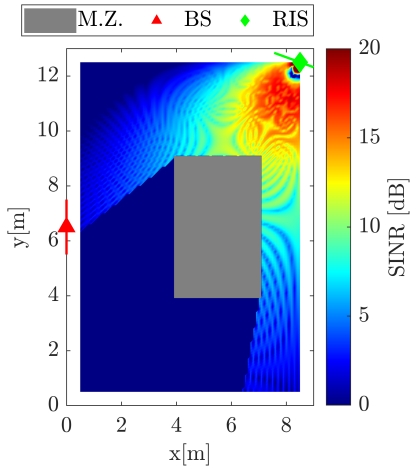

Fig. 3: Exemplary SINR distribution for the UE-RIS-BS links, when considering the upper RIS.

we leverage a predictive algorithm to forecast the occurrence of potential blockages, i.e., to estimate whether an obstruction will occur between the BS and any UEs within two radar updates. Specifically, each Kalman filter (see Sec. III) updates the state at each radar update, while in between two measurements, it predicts the state using a constant velocity model. Then, a linear interpolator considers the past five time instances to predict the machine's position at the next step, enabling the verification of potential blockages. Then, based on the current and predicted positions, the possibility of blockage events is assessed for each UE-machine pair. If a blockage is predicted, the network proactively activates the appropriate RIS[2] by selecting the proper phase shift vector $\psi_m(\Theta_{\text{inc}}, \Theta_{\text{ref}})$, to ensure stable communication for UEs that are expected to be obstructed before the next radar measurement. Since we consider only two RISs and assume that each RIS can serve at most one UE at a time, we adopt a greedy approach, prioritizing the UEs closest to the RISs. Similarly, the BS's multiple antenna is configured to direct its beam toward the newly activated RIS.

Based on this proactive configuration of both the BS and RISs, UEs perform uplink transmissions to the BS following an Unslotted Aloha Medium Access Control (MAC) layer protocol accounting for the propagation delay. In fact, at THz frequencies the propagation delay is typically in the same order of magnitude as the transmission time thus making useless any MAC relying on carrier sensing.

In particular, the MAC layer protocol works as follows. Whenever an UE has new DATA to be transmitted, it initiates a Back-Off (BO) phase for $T_{\text{B}} = T_{\text{BO}}\,\xi$, where T_{BO} is the minimum BO duration; ξ is a uniform random number in the range $[1; 2^i C]$, with C being an integer defining the duration of the contention window and i being an integer counting the number of transmission attempts (starting at 0 for the first attempt). At the end of the BO period, the UE sends the DATA and enters reception mode for a maximum period, T_{WAIT}. Specifically, we set $T_{\text{WAIT}} = T_{\text{ACK}} + 2\,\tau_{\text{p}_{\max}}$, since it is the time needed to receive the corresponding Acknowledgment (ACK), where $T_{\text{ACK}} = \frac{8\,P_{\text{A}}}{R_{\text{b}}}$, P_{A} is the number of bits forming an ACK, $R_{\text{b}} = B\log_2(M)$ is the bit rate (where we assume that the symbol rate equals the bandwidth), M is the modulation order considering an M-QAM modulation scheme, and $\tau_{\text{p}_{\max}}$ is the maximum possible propagation delay in the considered IIoT scenario. If an ACK is received during T_{WAIT}, the UE goes back to BO, as we consider the worst-case condition where all UEs have always a new DATA to be transmitted. Conversely, if no ACK is received during T_{WAIT}, the UE retries the transmission up to a maximum number of attempts, R.

The successful reception of a DATA or ACK transmission depends on the radio channel quality. For the k-th link, this quality is measured in terms of SINR_k, which is computed as in (4), based on the proactive configuration of the BS and RISs, updated every τ seconds. In this way, given a specific error correction code and coding rate $R_{\mathbf{c}}$, SINR_k is mapped to a packet error probability P_w[3]. A transmission is thereby considered successfully received if a randomly generated number between 0 and 1 exceeds P_w; otherwise, it is deemed lost.

Finally, to evaluate the overall network performance of our solution, we use the network throughput, defined as:

$$S = \frac{8PN_{\text{R}}}{T_{\text{S}}}, \tag{7}$$

where P is the number of bytes forming the DATA, N_{R} is the number of DATA successfully received at the BS within the simulation time T_{S}.

VI. Numerical Results

The proposed approach has been implemented in a custom MATLAB-Python simulator. While results refer to the scenario in Sec. II, the simulator and underlying model are scalable to more complex configurations with additional UEs, RISs, and dynamic machines. Simulation parameters, if not otherwise specified, are listed in Table I. Notably, to manage the huge number of RIS elements required to provide a reasonable link budget in NLoS condition, the simulator uses the large RIS approximation from [11], which significantly lowers the computational complexity when deriving the UE-RIS-BS channel. Additionally, each RIS element is modeled like a patch antenna, as detailed in [10].

To evaluate the overall effectiveness of our proposal, Fig. 4 depicts the network throughput as a function of the radar update interval within a simulation time of $T_{\text{S}} = 1$ ms. We compare our radar-based approach, applied using two configurations of receive antenna elements at the radar, namely $M_{\text{r}} = 32$ and $M_{\text{r}} = 128$, against an *oracle*-based approach that has perfect and continuous knowledge of obstacles and UEs positions. The performance of the latter, introduced here as a

[2]We assume ideal, instantaneous BS-RIS communication and a network with a-priori knowledge of RIS coordinates.

[3]For simplicity, we assume that each transmission consists of a single codeword.

TABLE I: Simulation parameters.

Parameter	Symbol	Value
Carrier frequency	f_c	300 GHz
Bandwidth	B	3 GHz
BS antenna element gain	G_n	0 dB
BS noise figure	N_F	8 dB
BS antenna elements	N_r	256×256
UE antenna element gain	G_k	0 dB
Transmit Power	P_t	0 dBm
RIS antenna elements	N_{ris}	128×128
Modulation order	M	4
Coding Rate (BCH code)	R_c	0.9
DATA size	P	20 B
Minimum Back-Off time	T_{BO}	13.3 ns
Simulation time	T_S	1 ms
ACK size	P_A	10 B
Maximum propagation delay	$\tau_{p_{max}}$	72.7 ns
Contention window	C	5
Maximum retransmission attempts	R	3

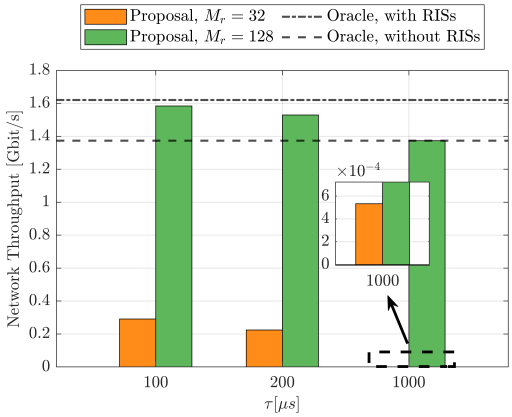

Fig. 4: Network throughput comparison between our solution and an ideal oracle, varying radar update periodicity (τ), number of radar receiving antennas (M_r), and RISs presence.

benchmark, has been evaluated with and without the presence of RISs in the scenario.

As expected, network throughput increases with more frequent radar updates, as this enhances the accuracy of proactive RISs activation, thereby reducing losses during obstruction events. Additionally, the performance deteriorates significantly when the radar has an insufficient number of receiving antennas due to inaccurate position estimation (see the curves for $M_r = 32$ and $M_r = 128$). Indeed, the performance of our approach matches that of the oracle without RISs only by setting $M_r = 128$. With a single radar update, $\tau = 1$ ms, the network acquires the estimated map only at the start of the simulation, preventing timely RISs activation and thereby resulting in performance far below that of the oracle with RISs. Conversely, with five and ten radar updates, i.e., $\tau = 200$ and $\tau = 100$ μs, respectively, our solution is able to closely approximate the ideal oracle, even when the oracle employs RISs as soon as needed.

VII. Conclusion

This paper has proposed an algorithm that dynamically and proactively configures a THz network (i.e., BS and RISs) based on centimeter-level sensing data obtained from a multi-antenna radar co-located with the BS. The proposed solution is validated through network-level simulations of uplink data traffic in a realistic, dynamic industrial environment and compared against an ideal oracle with perfect, continuous environmental knowledge. Numerical results show that our approach can closely match the oracle's network throughput when the radar has at least 128 receive antennas and generates radio maps with a periodicity of at most 100 μs.

Acknowledgment

This work has been performed in the framework of the HORIZON-JU-SNS-2022 project TIMES, cofunded by the European Union. Views and opinions expressed are however those of the authors only and do not necessarily reflect those of the European Union.

This work has been supported by the European Union - Next Generation EU under the Italian National Recovery and Resilience Plan (NRRP), Mission 4, Component 2, Investment 1.3, CUP F83C22001690001, partnership on "Telecommunications of the Future" (PE00000001 - program "RESTART").

References

[1] E. Sisinni, A. Saifullah, S. Han, U. Jennehag, and M. Gidlund, "Industrial internet of things: Challenges, opportunities, and directions," *IEEE Transactions on Industrial Informatics*, vol. 14, no. 11, pp. 4724–4734, 2018.

[2] ETSI, "TeraHertz modeling (THz); Identification of use cases for THz communication systems," *Group Report 001 v1.1.1*, 2024.

[3] E. N. Papasotiriou, A.-A. A. Boulogeorgos, and A. Alexiou, "On the impact of beam misalignment in reconfigurable intelligent surface assisted thz systems," in *2021 IEEE 22nd International Workshop on Signal Processing Advances in Wireless Communications (SPAWC)*, 2021, pp. 121–125.

[4] Y. Liu, X. Liu, X. Mu, T. Hou, J. Xu, M. Di Renzo, and N. Al-Dhahir, "Reconfigurable intelligent surfaces: Principles and opportunities," *IEEE Communications Surveys & Tutorials*, vol. 23, no. 3, pp. 1546–1577, 2021.

[5] Z. Chen, B. Ning, C. Han, Z. Tian, and S. Li, "Intelligent reflecting surface assisted terahertz communications toward 6g," *IEEE Wireless Communications*, vol. 28, no. 6, pp. 110–117, 2021.

[6] M. Rahim, G. Kaddoum, and T. N. Do, "Joint devices and irss association for terahertz communications in industrial iot networks," *IEEE Transactions on Green Communications and Networking*, vol. 8, no. 1, pp. 375–390, 2024.

[7] M. Ahmed, A. Wahid, W. U. Khan, F. Khan, A. Ihsan, Z. Ali, K. M. Rabie, T. Shongwe, and Z. Han, "A survey on ris advances in terahertz communications: Emerging paradigms and research frontiers," *IEEE Access*, vol. 12, pp. 173 867–173 901, 2024.

[8] H. Zhang, B. Di, K. Bian, Z. Han, H. V. Poor, and L. Song, "Toward ubiquitous sensing and localization with reconfigurable intelligent surfaces," *Proceedings of the IEEE*, vol. 110, no. 9, pp. 1401–1422, 2022.

[9] M. Ester, H.-P. Kriegel, J. Sander, X. Xu *et al.*, "A density-based algorithm for discovering clusters in large spatial databases with noise," in *kdd*, vol. 96, no. 34, 1996, pp. 226–231.

[10] D. Dardari and D. Massari, "Using metaprisms for performance improvement in wireless communications," *IEEE Transactions on Wireless Communications*, vol. 20, no. 5, pp. 3295–3307, 2021.

[11] M. Najafi, V. Jamali, R. Schober, and H. V. Poor, "Physics-based modeling and scalable optimization of large intelligent reflecting surfaces," *IEEE Transactions on Communications*, vol. 69, no. 4, pp. 2673–2691, 2021.